INTERNATIONAL JOURNAL OF HYDROGEN ENERGY 41 (2016) 10695–10706

Available online at www.sciencedirect.com

ScienceDirect

journal homepage: www.elsevier.com/locate/he

Biochar from pyrolysis of cellulose: An alternative catalyst support for the electro-oxidation of methanol

María Luz Nieva Lobos [a,b,1], Juan Manuel Sieben [c,1], Vanina Comignani [c], Marta Duarte [c], María Alicia Volpe [b], Elizabeth Laura Moyano [a,*]

[a] INFIQC, Departamento de Química Orgánica, Facultad de Ciencias Químicas, Universidad Nacional de Córdoba, Córdoba, Argentina

[b] Planta Piloto de Ingeniería Química, PLAPIQUI (UNS-CONICET), Bahía Blanca, Argentina

[c] Instituto de Ingeniería Electroquímica y Corrosión (INIEC) and CONICET, Universidad Nacional del Sur, Av. Alem 1253 - (B8000CPB) Bahía Blanca, Argentina

ARTICLE INFO

Article history:
Received 20 December 2015
Received in revised form
12 March 2016
Accepted 6 April 2016
Available online 18 May 2016

Keywords:
Biochar
Fast pyrolysis
Cellulose
Cu–Ru@Pt nanoparticles
Electrocatalyst
Methanol electro-oxidation

ABSTRACT

In the present study, the biochar produced by fast pyrolysis at 350 °C of untreated and acid-treated cellulose are evaluated as supports of Cu–Ru@Pt core-shell nanoparticles (2.9 –3.5 nm) for the electro-oxidation of methanol in acid media. Carbon materials and the supported core-shell nanoparticles were characterized by physicochemical and electrochemical techniques. Cyclic voltammetry and chronoamperometry were used to study the activity of the catalysts. The nanocatalyst supported onto the biochar from acid-treated cellulose exhibited high electroactive surface area (38 m^2/g) and high performance in the methanol electro-oxidation reaction, reaching TON values of 0.151 molec. (sites s)$^{-1}$ at 0.5 V. This contribution provides a new approach for the utilization of an inexpensive carbon material precursor as cellulose to design alternative catalytic systems and their emerging applications in electrocatalysis.

Introduction

Biochar, a carbonaceous material from biomass thermochemical conversion, has received increasing attention for use in several applications [1]. The most common biochar application is soil amendment to mitigate greenhouse gas emission and improve soil health, although the relationship between biochar properties and its applicability as a soil amendment is still not conclusive. Surface morphology, such as pore distribution, surface area and surface functionality, are key properties to effectively utilize biochar as catalysts and adsorbents. Thus, these carbonaceous materials with high electrical conductivity, porosity and stability can be used as an electrode material in fuel cells or supercapacitors [2].

* *Corresponding author*. Tel./fax: +54 3515353867.
E-mail address: lauramoy@fcq.unc.edu.ar (E.L. Moyano).
[1] These authors contributed equally to this work.
http://dx.doi.org/10.1016/j.ijhydene.2016.04.041

Various possibilities have been described for the functionalization of biochar materials for catalytic applications [3]. Generally, the functionalization of the carbonaceous surfaces can be directly performed *in situ* during the materials synthesis or through a post-synthetic modification where functional groups are introduced after preparing the carbonaceous supports.

Recently, nanostructured carbon materials, such as graphene nanosheets, carbon nanotubes, carbon arrays with ordered nanopores, between others, have been used as catalyst support in electrocatalytic processes. However, these materials are expensive and applications are restrictive in comparison with commercial Vulcan XC-72, although this material shows some limitations as low surface area, large quantities of micropores which are not suitable for an elevated mass transfer rate, and is susceptible to corrosion in fuel cell operating conditions. On the other hand, biomass-derived carbon materials are cheap and abundant, and can be easily prepared by a vast number of processes. In addition, high-ordered structure of carbonaceous materials providing high surface areas and malleable porosity can be produced from different biomass raw sources. In a previous work some of us, concluded that pyrolysis of microcrystalline cellulose (untreated or previously washed with acid) led to bio-oils with relatively high concentration of valuable anhydrosugars (mainly levoglucosan in the pyrolysis of MC and levoglucosenone) [4]. In this process, biochars were obtained as residual material of pyrolysis, which could be considered as supports for catalysts.

Biochars may thus effectively replace the commercial carbon-based catalysts in electrocatalytic applications. Major electrocatalysis applications of these biomass-derived carbons include methanol electro-oxidation [5] and oxygen reduction reaction (ORR) [6].

Methanol electro-oxidation is an electrical energy mediated chemical transformation which is the fundamental basis of direct methanol fuel cells (DMFCs). To improve the performance of DMFCs, some factors in the catalyst are considered such as electron conductivity, proton conductivity and mass transport. Carbonaceous materials have been used as catalyst supports because of their unique features such as high temperature stability, good resistance to acidic and basic media, and excellent electronic conductivity. It has been determined that the support plays a very important role in the size and distribution of the particles formed on its surface [7], and diffusion kinetics of reactants as well as products [8].

Carbon supported Pt-based electrocatalysts are commonly used in low temperature fuel cells [9,10]. Platinum is the best catalyst for alcohol oxidation. However, the high cost of platinum limits its use. Therefore, it is important to explore new metal-carbon nano-composite systems with high catalytic performances by searching for appropriate carbon sources and preparation methods of the catalysts. The use of carbon materials with high surface area as catalysts support improves catalysts performance and reduces the amounts of catalysts and thus their cost. Over the last few years, a huge number of new carbon materials have been developed and tested in order to enhance the electrochemical response of anode materials for direct methanol fuel cells. For instance, Lazaro et al. synthesized Pt and Pt–Ru nanoparticles supported over carbon nanocoils [11] carbon xerogels [12,13] and carbon nanofibers [14,15]. The authors found that Pt–Ru catalysts supported on nanocoils, nanofibers and xerogels develop higher activities during methanol oxidation than the commercial materials only when these novel carbon supports have a high electroactive surface area, an adequate number of oxygen functionalities and high methanol diffusion through their pores. Habibi et al. [16] and Chen et al. [17] synthesized carbon ceramic supported Pt–Ni particles and expanded graphite supported Pt–Co nanoparticles, respectively, and observed significant enhancement in the electrodes performance in comparison with Pt/C. Wang et al. [18] prepared graphitic carbon nanocapsules with high crystallinity and high specific surface area and used them as a promising material support for platinum nanoparticles. This electrode exhibited higher catalytic activity and improved stability for methanol oxidation compared with commercial Pt/C. Moreover, graphene [19] and graphene aerogels [20] were employed as catalyst supports for the electro-oxidation of methanol in acid and alkaline media. The enhanced catalytic activity of these electrodes was attributed to the highly porous structure and the highly conjugated sp^2-carbon network of graphene. A novel mesoporous catalyst-support material of vanadium carbide incorporated on resorcinol-formaldehyde resin carbon was developed by Li et al. [21]. The Pt-supported catalyst exhibited a higher current density, more negative onset-potential and slower degeneration rate than a commercial Pt/C-JM catalyst for methanol electro-oxidation. The authors concluded that the enhanced performance of the catalyst is due to high surface area of the mesoporous material and the synergistic effect between Pt and vanadium carbide. Jang et al. [22] fabricated multilayered metal/carbon hybrid nanostructures containing Pt and Pt–Ru by combining a layer-by-layer deposition process. They found that the carbon structures containing multilayers of highly dispersed Pt–Ru nanoparticles exhibit enhanced electrocatalytic activity in methanol oxidation.

Microcrystalline cellulose is as a model reactant of different lignocellulosic sources as agricultural residues, sugarcane bagasse and wood pulp. In this context, the cellulosic materials offer enormous potential to be used as a renewable feedstock with easy availability for the manufacture of cost-effective catalyst supports via fast pyrolysis. On the other hand, the most promising strategy to prepare cost-effective, durable and highly active catalyst with low Pt content involves the production of multimetallic particles with core-shell or pseudo core-shell architecture. In this study, the biochar produced by fast pyrolysis of untreated and acid-treated cellulose was evaluated as a carbon support of Cu–Ru core Pt shell nanoparticles. The supported pseudo core-shell nanoparticles synthesized by a two-step route were characterized by physicochemical and electrochemical techniques. The electro-oxidation of methanol in acid media was selected to investigate the properties of biochars as new catalyst support. The influence of the carbon support on the catalytic activity of the trimetallic nanoparticles was analyzed and the catalytic performance of the as-prepared electrodes compared to other Pt-based catalysts, with similar or higher Pt loading supported on conventional carbon materials.

Experimental

Cellulose samples

Cellulose (cotton linters) was directly purchased from Biopack. In the acid impregnation, microcrystalline cellulose (1.00 g) was treated with 5 ml of 5% (w/w) phosphoric acid (Anedra) aqueous solutions. The acid mixture was kept at 70–80 °C under continuous magnetic stirring during 2 h. After that, the mixture was filtered under vacuum and the cellulosic material was dried at 40 °C under vacuum overnight.

Both cellulose materials were characterized by X-ray diffraction (XRD) using a Philips PW1710 BASED instrument operating at 45 kV and 30 mA, fitted with a graphite monochromator in order to get Cu Kα1 radiation (λ = 1.5406 Å). Crystallinity index of microcrystalline and pre-treated cellulose was calculated based on the data of X-ray diffractometry [23]. Besides, these materials were studied by Scanning Electron Microscopy (SEM) on a JEOL 100 CXII apparatus.

Pyrolysis experiments

The fast pyrolysis of cellulose was carried out in a horizontal flow reactor under nitrogen flow of 0.06 L min^{-1} in a temperature range of 250–500 °C. The pyrolysis unit consisted of a feeding system, a vacuum pyrolysis system, and a condensation system, as previously described in Refs. [4,24]. Cellulose samples (1.00 g) were crushed and sieved to obtain particles of 10–20 mesh size and placed in a sliding quartz boat, which was fed into the pyrolysis furnace when temperature and vacuum settings were reached and kept at these conditions for 20 min.

After the experiments were completed, the pyrolyzate was extracted from the condenser with organic solvents. The yield of the liquid and char products was calculated by the weight difference of the condenser and the quartz boat, respectively, before and after the experiment. The yield of gas was calculated by the difference of starting cellulose and generated pyrolysis oil and char. All yields are informed as the average of at least three experiments to verify the reproducibility of the reported results.

The solid chars employed in this work were characterized in order to determine several physicochemical properties: crystallinity (XRD), specific surface area (BET), scanning electron microscopy (SEM), thermo-gravimetrical analysis (TGA) and infrared spectroscopy (FT-IR). P content of biochars was determined by ICP in a (ICP-OES) Shimadzu 9000 apparatus.

X-Ray diffraction patterns were recorded in a Panalytical X'Pert Pro instrument (40 mV, 40 mA), using a Cu Kα (λ = 1.5418 Å) radiation and graphite monochromator. The data were collected in the 2θ range: 5.0175–59.9675°, the scanning step was 0.035°, with a scan step time of 2 s per point. Lattice parameters and crystallite size were determined by Rietveld analysis.

Nitrogen isotherms were determined at −196 °C using a Nova 1200e Quantachrome instrument after degassing the produced chars at 150 °C until outgassing was completed. BET equation was used for surface area calculations.

TG runs were carried out with a Shimadzu DTG 60 on samples of around 5 mg under nitrogen and synthetic air (N_2:O_2 4:1) environments, using a heating rate of 10 °C min^{-1} from 25 to 1000 °C.

Fourier Transform Infrared (FTIR) spectroscopic analysis of all samples was performed using a FTIR Bruker IFS 28v spectrometer, with a resolution of 2 cm^{-1} in the range of 4000–400 cm^{-1} by using KBr disks.

Catalyst preparation

The carbon materials derived from pyrolysis of microcrystalline cellulose and phosphoric acid-treated cellulose samples were used as supports for the preparation of Cu-Ru@Pt core-shell electrocatalysts (PRC/BMC and PRC/BTC catalysts). The Cu-Ru@Pt core-shell nanoparticles were synthesized through a two-step method. First, adequate amounts of the metal salts, $CuSO_4$ and $RuCl_3$, were dissolved in a sodium citrate/citric acid buffer solution (pH = 3) at room temperature. After that, 50 ml of aqueous biochar dispersion was added (2 mg mL^{-1}) and sonicated for 30 min. The Cu–Ru nanoparticles supported on the carbonaceous materials were formed by reduction of the salts with $NaBH_4$ in a weight ratio of 3:1 to metals under moderate stirring for 2 h and then collected via suction filtration, washed repeatedly with bidistilled water and ethanol and re-dispersed in 50 ml of bidistilled water.

Finally, the Cu-Ru@Pt core-shell nanoparticles were obtained by the spontaneous galvanic replacement reaction of Cu atoms by Pt^{4+} ions. The reaction was conducted for 2 h by adding a very dilute aqueous solution of H_2PtCl_6 to the CuRu/biochar dispersion under vigorous magnetic stirring at room temperature. Thereafter, core-shell catalysts supported on the biochars were collected by suction filtration, washed with water and ethanol and dried at 70 °C for 12 h.

Electrochemical characterization

All the electrochemical experiments were carried out in three-compartment glass cells with a PAR 273 potentiostat/galvanostat controlled using M270 software. The counter electrode was a platinum wire and a saturated calomel electrode (SCE, +0.241 V vs. RHE) located in a Luggin capillary served as the reference electrode. The working electrodes were prepared by dispersing 20 μL of a catalyst ink over glassy carbon rod electrodes (3 mm diameter). The catalyst ink was made by following the procedure described in a previous paper [25]. Electrochemical techniques such as cyclic voltammetry (CV) and chronoamperometry (CA) were used to evaluate the catalysts. An inert N_2 atmosphere was maintained over the solution during the electrochemical tests. Potentiodynamic experiments were conducted at a sweep rate of 50 mV s^{-1} in 0.5 M H_2SO_4 solution. The electroactive surface area of the supported catalysts was determined by Cu-UPD technique, following the procedure described elsewhere [26]. The electrocatalytic performance of biochar supported trimetallic nanoparticles towards methanol oxidation (1 M MeOH) in acid media (0.5 M H_2SO_4) was evaluated by CV (40 cycles) at 50 mV s^{-1} and potentiostatic experiments at different potentials (0.3–0.6 V). Catalytic activities were normalized in terms of current per unit of active surface area and current per mass of Pt.

Physicochemical characterization

The catalysts were characterized using Transmission Electronic Microscopes, TEM, JEOL 100CX II and JEOL JEM-2010 operated at 200 keV. The samples for TEM analysis were prepared by putting a drop of the catalyst ink on a standard copper grid. EDX analysis of the materials was performed by an energy dispersive X-ray spectroscopy probe attached to a scanning electron microscope (SEM, JEOL 100). The samples were supported on mirror-polished GC disks and the analysis was done in five different zones with the incident electron beam energies ranging from 0.1 to 20 keV. X-ray diffractograms (XRD) of the synthesized materials were recorded using a Rigaku Dmax III C diffractometer with monochromated CuKα radiation source operated at 40 keV at a scan rate of 0.05° s^{-1}. Lattice parameters and crystallite size were determined by Rietveld analysis. Moreover, the loading of the metals deposited on the carbon substrate was determined by ICP-AES (Shimadzu 1000 model III) analysis. The platinum loading of the samples expressed per unit of GC geometric area was $50.5 \pm 3.5\ \mu g\ cm^{-2}$. The total metal (Pt + Cu + Ru) loading of the catalysts was 11.3 ± 1.5 wt. %.

Results and discussion

Characterization of cellulose materials

Microcrystalline cellulose (from now on MC) and cellulose impregnated with phosphoric acid (from now on TC) were analyzed by XRD diffraction. Fig. 1 clearly shows that the diffraction peaks of cellulose crystals were observed in both cases. From these diffractograms the crystalline index determined for MC was 81% while a value of 69 % was obtained for TC. Thus, for TC, it was observed that an effective reduced number of ordered micro-regions of the cellulose polymer increased the relative content of amorphous regions, which is in agreement with previous studies [27,28].

The morphologic modification of MC after acid treatment was previously investigated by SEM analysis indicating that cellulose ribbons are clearly observed for microcrystalline cellulose together with amorphous regions [4]. After treatment, cellulose material consisted of a very large amount of agglomerates where fibers are distinctly reduced in length compared with MC showed many terraces, steps and kinks. This morphologic alteration can be attributed to the surface dehydration of the polymer, which is effectively catalyzed by the acid [29].

Fast pyrolysis of cellulose samples

Pyrolysis experiments of MC and TC were carried out at different temperatures: 250, 300, 350, 400 and 500 °C. Conversion of MC to products was achieved at temperatures higher than 200 °C and the liquid fraction increased with the increase of temperatures giving good yields (54%) at 400 °C, while solid fraction or biochar decreased from 69 % at 250 °C to only 3 % at 500 °C (Fig. 2). Gaseous products were predominant between 300 and 350 °C reaching 56 % at 350 °C and its formation was moderate at higher temperature.

On the other hand, the treatment of cellulose with phosphoric acid favored the formation of biochar (25–44 %) at the expense of liquid products (5–10 %) [4]. As in the case of pyrolysis of MC, the gas fraction was the main product in these experiments (52–65 %).

Biochar typically accounts for 10–80 % yields, different chemical treatments (washing/leaching) of starting cellulosic materials can promote the formation of biochar and volatile compounds at the expense of bio-oils, the product distribution is strongly dependent on the biomass type, reaction and pretreatment conditions [1,4,30].

Characterization of biochar

The carbonaceous solids produced in the pyrolysis of microcrystalline cellulose (named BMC) and acid-treated cellulose (named BTC) at 350 °C, obtained in 6 and 40 % yield respectively, were selected as supports for the preparation of Cu-Ru@Pt core-shell electrocatalysts (PRC/BMC and PRC/BTC catalysts). The biochars obtained at lower temperature were disregarded mainly due to the low carbon content as well as the high hydrogen and oxygen content, however; the

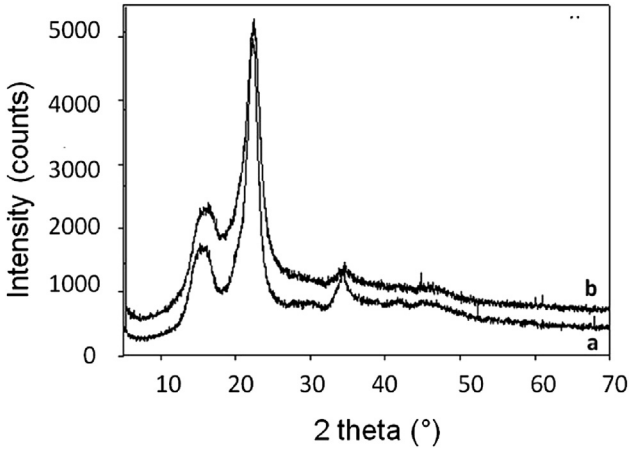

Fig. 1 – XRD patterns of microcrystalline cellulose (a) and of acid treated cellulose (b).

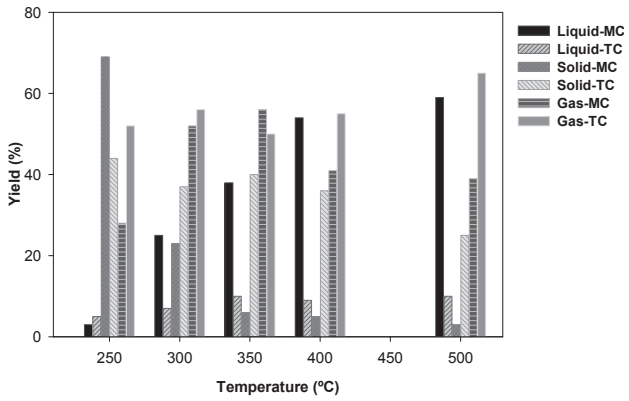

Fig. 2 – Product yields (liquid, solid and gas) in the fast pyrolysis of microcrystalline cellulose (MC) and acid-treated cellulose (TC).

carbonaceous materials obtained at 350 °C displayed high carbon content (Table 1), which is desirable for the catalyst supports required for the electro-oxidation reaction here studied. In addition, the phosphoric acid treatment of starting cellulose resulted in a carbon enhanced solid with low content of O and traces of remaining P. On the other hand, analyses of biochars were conducted by running adsorption isotherms of adsorption–desorption of N_2 at −196 °C, calculating the BET surface area, and measuring pore volume and size (Table 1).

BMC displayed relatively small BET surface area indicating that only a few number of pores were generated during the fast pyrolysis because of the incomplete pyrolysis of cellulose, low temperature and the entrapment of tar-like materials within the pores. Biochar obtained from pyrolysis of TC showed a BET surface area higher than the biochar generated in the reactions of MC. This increase in BET surface area can be attributed to the effect of phosphoric acid in the dehydration of the starting biopolymer which produced pores and less ordered micro-regions in the final solid. It is known that chemical acid activation of cellulosic materials promotes the release of volatile compounds due to dehydration, thus the decrease of crystal structure caused by the acid facilitated the enlargement of the existing pores and the generation of new ones [31]. Average pore diameter of biochars was 3.0 and 2.4 nm, for BMC and BTC respectively. Most of the generated pores in BTC had smaller size than BMC although BTC displayed a high total pore volume. Regarding pore size distribution, it was observed that for both biochars a small fraction (1–3 %) of the pores showed sizes of mesopores. Thus both BMC and BTC should be considered mainly as microporous materials.

The XRD patterns of biochars showed two broad diffraction peaks corresponding to the characteristics peaks of carbon (Fig. 3). The strongest peak located at $2\theta = 20–30$ ° is attributed to the amorphous carbon structure while the weaker diffraction peak at around $2\theta = 40–50$ ° is assigned to the reflection from graphite [32]. Graphitic structures are commonly observed in biochars obtained from pyrolysis carried out at temperatures much higher (700–900 °C) than the one employed in the present study (350 °C). However; traditionally lignocellulosic biomass is employed for obtaining biochars at high temperatures. The starting material (microcrystalline cellulose) could originate low amount of graphite even at relatively low pyrolysis temperature, since the absence of lignin strongly modifies the thermal lability of the sample.

FT-IR spectra obtained with biochars BMC and BTC are presented in Fig. 4. For BMC (Fig. 4a), the broad band at 3234–3551 cm^{-1} was associated with O–H stretching vibration mode of hydroxyl functional groups of alcohols, acids and phenols. It can be observed a broad and weak peak at 2990–2820 cm^{-1} corresponding to aliphatic and aromatic

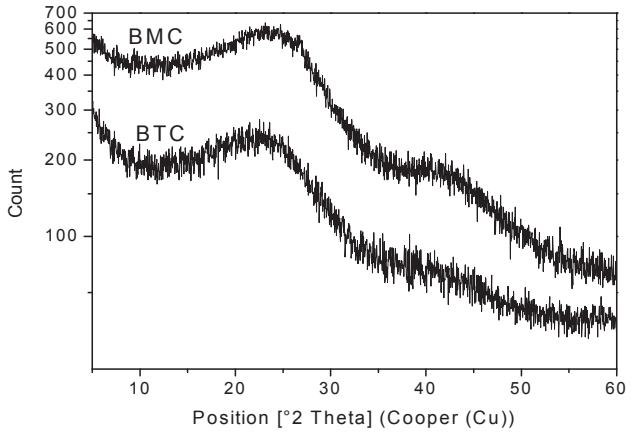

Fig. 3 – XRD patterns of biochars BMC and BTC.

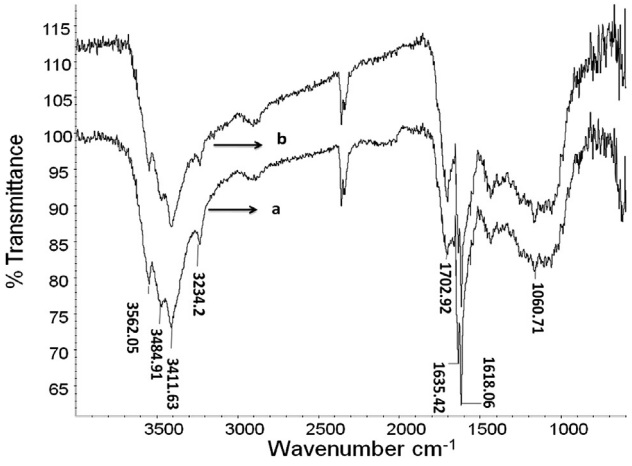

Fig. 4 – FT-IR spectra of biochars: (a) BMC and (b) BTC.

asymmetric C–H and symmetric C–H stretching bands. The bands between 1000 and 1750 cm^{-1} showed the presence of oxygen containing functional groups. For example, the band at 1707 cm^{-1} was ascribed to C=O vibrations in carbonyl groups and the broad bands at 1165 and 1061 cm^{-1} can be assigned to the C–O stretching vibrations that indicates the presence of aromatic alcohols and/or ethers. The strong absorption bands between 1640 and 1580 cm^{-1} can be assigned to C=C vibrations present in olefinic vibrations in aromatic region. As compared to BMC (Fig. 4a) and BTC (Fig. 4b), main FT-IR bands presented similar frequency absorption and intensity.

These results showed that there was no significant difference in the surface functional groups between biochar derived from pure cellulose and acid-treated cellulose.

Table 1 – Physicochemical properties of biochars

Samples	S_{BET} ($m^2\ g^{-1}$)	V_{TPore} ($cm^3\ g^{-1}$)	D_{pore} (nm)	C (wt. %)	H (wt. %)	N (wt. %)	O[a] (wt. %)	P (wt. %)
BMC	199	0.0264	3.0	58.42	2.88	0.07	36.13	ND[b]
BTC	557	0.22	2.4	70.56	3.54	0.13	23.66	0.21

[a] Calculated by difference taking into account the ash content.
[b] Not detected.

TGA and DTG data demonstrate a continuous mass loss associated with increasing temperature (Fig. 5), which was attributed to the breaking of chemical linkages and removal of volatile products from both biochars. There were two possible steps of mass loss occurring in BMC with significant mass loss phases at 50–150 °C and 380–600 °C (Fig. 5a), mainly due to decomposition of oxygen containing functional groups (H_2O, CO_2 and CO, Table 2).

The carbonization process of this biochar was completed around 600 °C since all oxygen containing groups were eliminated from biochar at this temperature. TGA results of BTC (Fig. 5b) were not significantly different from BMC. The highest mass loss (75 wt. %) occurred from 450 °C, which was about 13 wt. % lower than that of BMC at similar temperature range. In this case it was observed two step of mass loss at high temperature, one at 450–650 °C and other at 680–750 °C. For this material the carbonization was completed at 750 °C, at higher temperatures that BMC. These results would indicate a thermal stabilization in the biochar originated from acid-treated cellulose, which induce a delayed carbonization of the material [33].

Biochar supported Cu–Ru@Pt catalysts

Physicochemical characterization

Table 3 shows the atomic ratios determined by EDX, the average diameter of the nanoparticles (d_p), as well as the specific surface area of both catalysts. According to these results the composition of the trimetallic core-shell system depends on the presence of functional oxygenated groups and surface defects (i.e. terraces, steps and kinks). Similar results have been reported elsewhere [13,34,35]. As was mentioned in a previous report, the interface is strongly distorted when the carbonaceous material is activated and this surface modification can change the real potential of the electrode, modifying the conditions for ruthenium and copper deposition [34]. In other words, the activation process leads to a change in the work function of the carbonaceous material which in turns influences the catalyst precursors–support interaction.

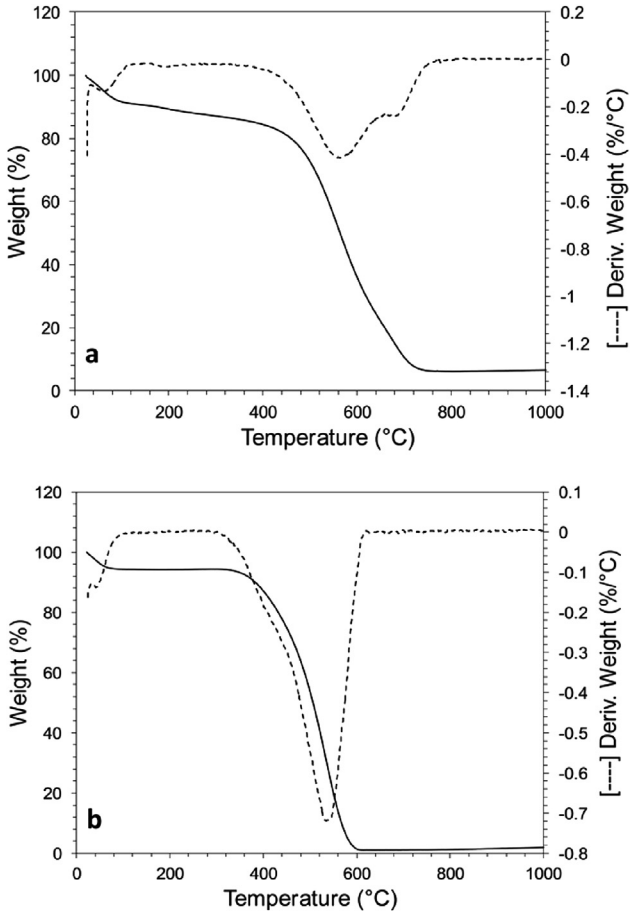

Fig. 5 – TG-DTG analysis of (a) BMC and (b) BTC.

Table 2 – Biochar composition based on temperature of mass loss.

Sample	Interval of integration °C	Weight loss %	Mass loss (mg)[a]	Products
BMC	20–100	10	0.52	H_2O
	350–600	88	4.69	CO_2–CO
BTC	50–200	20	1.20	H_2O
	450–750	75	4.46	CO_2–CO

[a] Initial mass for BMC: 5.28 mg and BTC: 5.95 mg.

Fig. 6 shows the TEM micrographies of the core-shell nanoparticles supported on biochar carbons and their respective histograms of particle size distribution. The analysis indicated that the nanoparticles are nearly spherical with diameters in the range of 2–5 nm. The nanoparticles of PRC/BMC have a mean particle size of 3.5 ± 0.7 nm, while the nanoparticles observed in the TEM image of PRC/BTC catalyst have a mean diameter of 2.9 ± 0.5 nm. Some agglomerates of about 15 nm can be observed in the micrographies and both catalysts exhibit narrow particle size distributions.

The electroactive surface area (ESA) of the PRC/BTC was in the order of 38 $m^2\ g^{-1}$, while the ESA value of PRC/BMC was about half of that corresponding for PRC/BTC. As can be noted from the above results, the phosphoric acid activation of the biochar carbon material has an important influence on particle size and on dispersion, since the presence of surface defects enhances the adsorption of the catalyst precursors. In other words, the structural defects (i.e., terraces, steps and kinks) behave as nucleation centers or anchoring sites for particle formation [13,34]. Due to the fact that BTC shows a much larger specific surface area than BMC, the concentration of such defects is higher for the former than for the latter biochar. Thus, BTC promotes the dispersion of the catalyst precursor in a higher extend than BMC does.

Fig. 7 presents the X-ray diffraction patterns of the as-synthesized electrode materials. The diffractograms exhibit the characteristic peaks of the face-centered cubic (fcc) lattice structure of Pt, but the peaks appear shifted towards higher Bragg angles with respect to pure Pt, suggesting alloying between Pt, Cu and Ru. The (111), (200) and (220) reflections of platinum are located at 2θ values of 40.24 °, 46.13 ° and 69.33 ° for PRC/BMC (with d-spacings of 0.2240, 0.1966 and 0.1354 nm), and 40.43 °, 47.06 ° and 68.72 ° for PRC/BTC catalyst (with d-spacings of 0.2229, 0.1929 and 0.1365 nm). Such slight shift to higher 2θ angles could have to do with the difference in composition between PRC/BTC and PRC/BMC catalysts.

Table 3 – Composition and characteristic parameters of Cu-Ru@Pt catalysts.

Catalyst/ Biochar	Pt[a] (at.%)	Ru[a] (at.%)	Cu[a] (at.%)	Pt:Ru Ratio	d_p[b] (nm)	ESA[c] ($m^2 g_{Pt}^{-1}$)	d_c[d] (nm)	a_{fcc} (nm)
PRC/BMC	46.8	32.3	20.9	1.45	3.5	16.7	2.9	0.3844
PRC/BTC	43.1	41.9	15.0	1.03	2.9	37.6	2.6	0.3861

[a] Atomic composition from EDX analysis (±1.7 at.%).
[b] Mean particle size from TEM.
[c] Electroactive surface area per unit mass (±2.0 $m^2 g^{-1}$).
[d] Crystallite size estimated using Scherrer's equation.

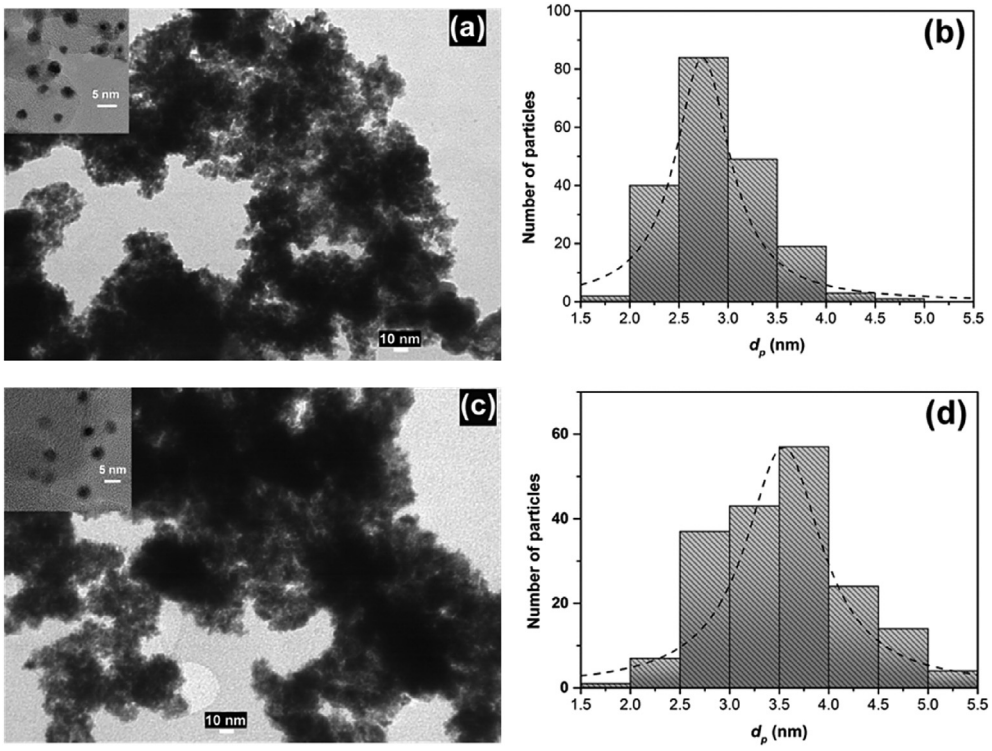

Fig. 6 – TEM images and histograms of particle size distribution of PRC/BTC (a) and (b) and PRC/BMC (c) and (d).

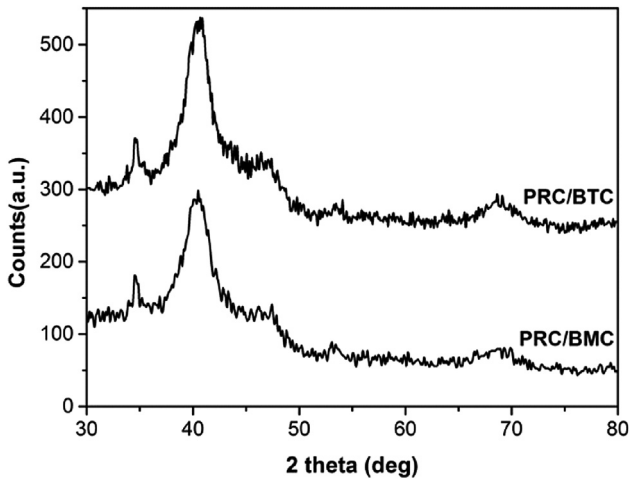

Fig. 7 – XRD patterns of Cu-Ru@Pt nanoparticles supported on the biochar materials.

Furthermore, no peaks indicating the presence of either hcp Ru phase, fcc Cu phase or ruthenium and cupper oxides are observed.

The crystallite size (d_c) calculated from the (111) and (220) reflections of Pt according to Scherrer's formula [36] and the lattice parameters of the samples are included in Table 3. The XRD results agree reasonably well with those determined from TEM analysis. Moreover, the lattice parameter shows the extent of lattice contraction arising from the replacement of the smaller Cu and Ru atoms for the bigger Pt atoms. Besides, the lattice strain of the Cu–Ru rich core in the Pt rich shell can also contribute to the change in the lattice parameter.

The latter could indicate that the Cu–Ru rich core nanoparticles were surrounded by a platinum rich shell (i.e., pseudo core-shell structure), in accordance with our previous results [24,37]. This structure is the consequence of the spontaneous inter-diffusion between the different metal atoms forming the small nanoparticles after the partial galvanic replacement reaction. The presence of vacancy

defects at the interface between the Cu–Ru core and the platinum shell may cause the alloying process [38].

Electrochemical characterization

The cyclic voltammograms of the biochar supported Cu-Ru@Pt catalysts in 0.5 M H_2SO_4 solution are shown in Fig. 8. The potentiodynamic curves do not show the presence of anodic/cathodic peaks related to Cu dissolution from the carbon supported trimetallic catalysts, suggesting that the Cu–Ru core is completely encapsulated by at least an uniform Pt monolayer. This behavior is very similar to those obtained for other nanostructured Cu rich core Pt rich shell trimetallic electrodes reported in a previous paper [37]. Moreover, the potential region between −0.25 and 0.0 V shows the characteristic feature of the bimetallic Pt–Ru catalysts, with a no well resolved hydrogen region as well as a cathodic wave at ca. 0.0 V associated with the reversible adsorption of OH species on Ru atoms [25]. This result is consistent with the results of the XRD analysis.

On the other hand, the figure also shows that the charge of the double-layer in the CV curve of PRC/BTC electrode is about four times higher than that of PRC/BMC. This difference can be explaining in terms of the better textural properties of BTC. The acid treatment of microcrystalline cellulose led to the development of extensive porosity within the carbon material structure. Such observations are confirmed by the calculated BET surface area and pore volume values (see Table 1).

Methanol electro-oxidation

Fig. 9 presents the cyclic voltammograms for methanol electro-oxidation at the as-prepared PRC/BMC and PRC/BTC electrodes at room temperature. For PRC/BTC electrode the onset for methanol electro-oxidation seems to take place at 0.27 V, while the onset potential is shifted to 0.38 V for PRC/BMC electrode. The electrocatalytic activity of PRC/BTC is four times higher than that of PRC/BMC in the potential region between 0.3 and 0.5 V but for potentials near the peak this difference is diminished by about 25 %. The peak current densities of methanol oxidation were 228 mA mg^{-1} (0.61 mA cm^{-2}) and 71 mA mg^{-1} (0.42 mA cm^{-2}) on the trimetallic catalysts supported over BTC and BMC, respectively. It can be noted that the enhanced electrocatalytic activity and the lower onset potential of the trimetallic nanoparticles supported on BTC is strongly associated with the high specific surface area and concomitantly with the high amount of surface defects that are present on the surface of this biochar carbon support, which in turn allows a smaller average particle size and a better distribution of the core-shell nanoparticles over this biochar support.

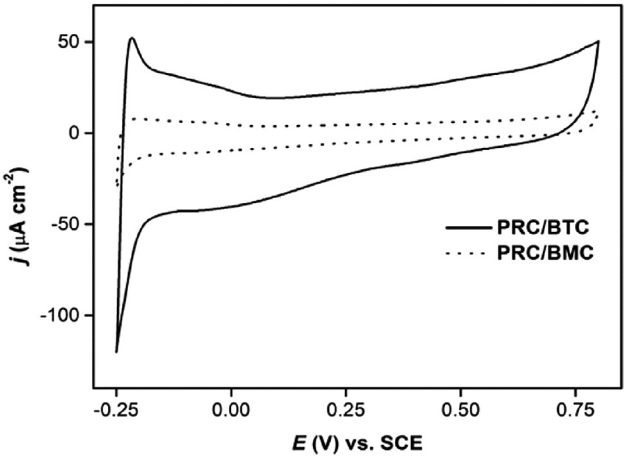

Fig. 8 – Cyclic voltammetry curves of Cu-Ru@Pt/BTC and Cu-Ru@Pt/BMC electrodes in 0.5 M H_2SO_4 solution at room temperature. Sweep rate 50 mV s^{-1}.

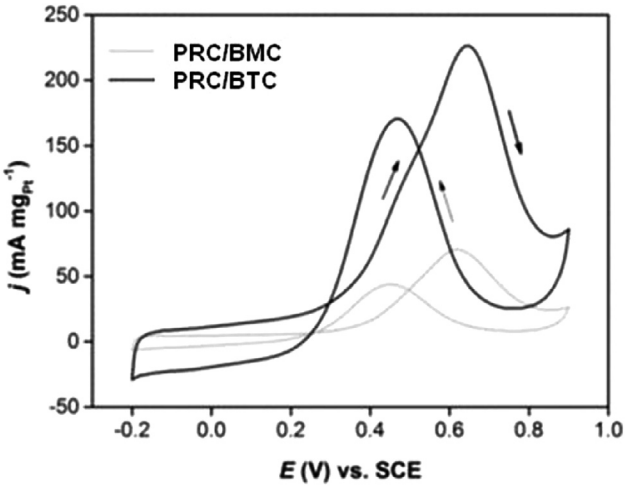

Fig. 9 – Cyclic voltammograms for the electro-oxidation of methanol in a 1 M CH_3OH/0.5 M H_2SO_4 solution at the different biochar supported catalysts. $\nu = 50$ mV s^{-1}.

Taking into account the microporous nature of the catalysts, diffusional mass limitation could play a role in the electro-oxidation reaction. Taking into account that the pores are larger for BMC than for BTC, it should be expected that if diffusion limitations ever take place, they would be higher for BTC (with smaller pores) than for BMC. With this in mind, the conclusion that TON value was much higher for BTC than for BMC (one order of magnitude for 0.5 V and more than three times higher for 0.4 V, see Table 4) stands in spite of the appearance of mass transfer limitation in BTC.

Potentiostatic experiments at different potentials were also carried out in order to assess the stability and poisoning rate of the biochar supported catalysts. Fig. 10a shows the chronoamperometric curves of the electrode materials at 0.4 V, and Fig. 10b compiles the electrocatalytic activities per milligram of Pt and per cm^2 of electrochemical area at different potentials. It can be observed that the catalytic activity of methanol oxidation for both electrodes increases up to 0.5 V and then falls off as a consequence of the accumulation of strongly adsorbed intermediates on the catalyst surface [39]. In this case, the catalytic activity of PRC/BTC is 5, 9 and 12 times higher than that of PRC/BMC at 0.3 V, 0.4 V and 0.5 V, respectively. The discrepancy between the results of cyclic voltammetry and chronoamperometric experiments may be attributed to significant differences in the extent of CO_{ad} accumulation on the PRC/BMC sample.

On the other hand, the catalytic activity of PRC/BTC is compared with the activity of a commercial Pt–Ru/C catalyst

Table 4 – Poisoning rate and turnover number of PRC/BMC and PRC/BTC electrodes for MOR at different potentials.

Catalyst/Biochar	0.4 V		0.5 V	
	δ	TON	δ	TON
	% s^{-1}	molec. $site^{-1}$ s^{-1}	% s^{-1}	molec. $site^{-1}$ s^{-1}
PRC/BMC	0.044	0.021	0.048	0.029
PRC/BTC	0.024	0.079	0.026	0.151

reported in our previous report (20 wt. % Pt + 10 wt. % Ru, $d_p = 2.9$ nm and $ESA = 60.3\ m^2\ g^{-1}$) [37]. The catalytic activity of the as-prepared catalyst is 9 and 3 times compared with the commercial system at 0.4 V and 0.5 V, respectively. This difference could be explained in terms of the electronic and strain effect that appears when the nanoparticles have a core-shell structure as well as the changes in the d-band of the Pt-rich shell caused by their interaction with the highly defective surface of the biochar carbon support. We ascribe the superior catalytic performance of PRC/BTC electrode mainly to the pseudo core-shell structure of the nanoparticles. According to theoretical analysis and experimental studies the compressive strain in the shell and the ligand effects caused by the atomic vicinity of two dissimilar metal atoms induces a downward shift of the d-band of Pt and pull more of the anti-bonding states below the Fermi level, which results in increasing occupation and weaker adsorbate bonding [40–42]. Goto et al. [41] concluded that Ru cores electronically modify surface Pt atoms to weaken Pt–CO bonding on Ru@Pt nanoparticles. While Strasser et al. [40] found that the compressive strain rather than ligand effects is responsible for the exceptional reactivity of Cu@Pt nanoparticles. Chen et al. [43] indicated that the enhanced electroactivity for methanol oxidation of Ru@Pt can be attributed to the compressive strain caused by the lattice mismatch between the Pt shell and the Ru core.

In order to complete the information on the performance of the trimetallic catalysts supported over the biochar carbons, the poisoning rate and the turnover number have been calculated. The poisoning rate was determined according to Equation (1) [44]:

$$\delta = \frac{100}{I_0}\left(\frac{dI}{dt}\right)_{t>500\ s} \quad (1)$$

where $(dI/dt)_{t>500}$ is the slope of the linear part of the current–time curve (A s^{-1}) and I_0 is the current determined from the intercept of the regression line with the y-axis (A).

Furthermore, the turnover number (TON) was determined according to the following expression [45]:

$$TON\left(\frac{molecules}{site\ s}\right) = \frac{j\,N_A}{n\,F\,1.3x10^{15}} \quad (2)$$

where, N_A and F have their usual meaning, j is the current density measured at 900 s (A cm^{-2}), n is the number of electrons generated when one methanol molecule is oxidized to CO_2 and 1.30×10^{15} is the number of surface platinum atoms taking part in the alcohol oxidation reaction [46].

The values of the poisoning rate and the turnover number for the methanol oxidation reaction at 0.4 and 0.5 V are collected in Table 4. It can be observed that the poisoning rate of the pseudo core-shell nanoparticles is reduced by half when the biochar support is activated with phosphoric acid. Moreover, the poisoning rate remains almost constant when the potential is increased. The latter behavior agrees well with the results reported elsewhere [24]. On the other hand, the turnover number of PRC/BTC is between 4 and 5 times higher than that of PRC/BMC. It is interesting to note that the improvement of the TON parameter with the applied potential is more noticeable in the trimetallic catalyst supported on the biochar-BTC. The TON value is twice as high as that at 0.4 V for PRC/BTC, while it only increases by about 14 % with the applied potential for PRC/BMC. Overall, the as-synthesized PRC/BTC electrode is able to catalyze the oxidation of methanol more efficiently than PRC/BMC. The faster turnover rate and the higher poisoning tolerance of the biochar-TC supported Cu-Ru@Pt nanoparticles can be satisfactorily explained in terms of the high amount of structural defects at the surface of this carbon that facilitates the oxidation of the poisoning species strongly adsorbed at the surface of the core-shell nanoparticles, either by providing OH_{ad} species (i.e., bifunctional mechanism) or by modifying the surface electronic structure of platinum [34,47,48].

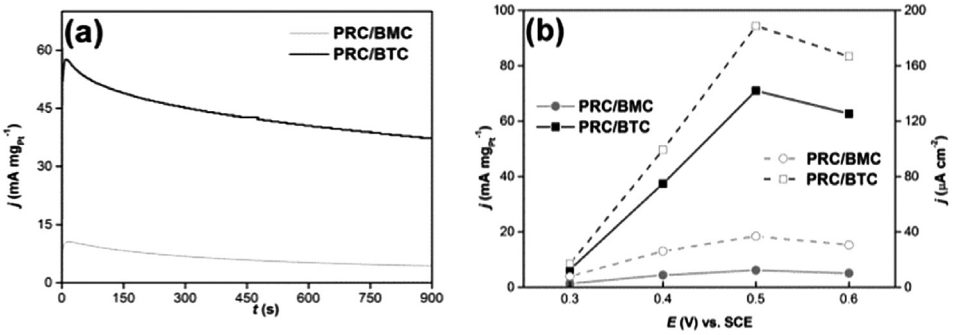

Fig. 10 – Current-time curves at 0.4 V (a) and catalytic activities at different potentials normalized with the Pt loading and the electroactive surface area (b) for PRC/BTC and PRC/BMC in a 1 M CH_3OH + 0.5 M H_2SO_4 solution.

The electrocatalytic performance obtained for the biochar BTC supported trimetallic Cu-Ru@Pt material is promising when compared to several electrocatalysts, with similar or higher Pt loading, supported over conventional carbon materials reported in the literature such as carbon nanotube buckypapers [35], carbon xerogels [49], mesoporous carbons [50–54], carbon nanofibers [55] and carbon black [56]. For instance, Su et al. [52–54] prepared and characterized Pt and Pt–Ru nanoparticles supported on different porous N-doped carbon materials. They reported catalytic activities between 250 and 350 A mg^{-1} for catalysts with 40 wt. % Pt and carbon supports with BET surface areas of about 1200 $m^2\ g^{-1}$. Meanwhile, Sebastián et al. [55] reported peak current densities in the range of 200–250 mA mg^{-1} for catalysts with Pt loadings of 20 wt. % and carbon nanofibers with BET areas between 120 and 185 $m^2\ g^{-1}$. While Calderón et al. reported catalytic activities between 100 and 300 mA mg^{-1} for Pt–Ru catalysts (20 wt. %) supported over carbon xerogels of BET surface areas of around 600–750 $m^2\ g^{-1}$ [13,14].

Moreover our electrocatalyst is also very competitive when compared with platinum catalysts supported over other biomass based carbon materials. Zhou et al. [57] synthesized a mesoporous carbon (ODC) with a BET surface area of 840 $m^2\ g^{-1}$ from okara pulp (a byproduct from soymilk and tofu production) and used it as support of Pt nanoparticles. The authors reported a peak current density of 294 mA mg^{-1} for the Pt/OCD catalyst made of nanoparticles having an average size equal to 3 nm, an ESA of 58.2 $m^2\ g^{-1}$ and 20 wt. % Pt loading. While Fang et al. [58] prepared porous carbon spheres (BET surface area = 2440 $m^2\ g^{-1}$) from pectin as support materials for Pt electrocatalysts. They reported a peak current density of 450 mA mg^{-1} and a catalytic activity of 50 mA mg^{-1} at 0.65 V vs. SCE with a catalyst made of Pt nanowires of 3 nm in diameter and 50 nm in length, a specific surface area of 55.6 $m^2\ g^{-1}$ and c.a. 23 wt. % Pt loading.

Conclusions

Carbonaceous materials easily produced from the fast pyrolysis of cellulose were efficiently used as catalyst support in the electro-oxidation of methanol.

Cu–Ru@Pt nanoparticles were supported on two different biochars, BMC and BTC, BMC produced from pyrolysis of microcrystalline cellulose while BTC was obtained from pyrolysis of acid-treated cellulose. The electrocatalytic behavior observed for BTC supported trimetallic catalyst is promising when compared to other electrocatalysts, with similar or higher Pt loading using conventional carbon material supports.

The present study confirms that the biochar derived from acid-impregnated cellulose is a promising support material for direct methanol fuel cells (DMFCs). These results encourage us to evaluate the performance of other biochars, especially those deriving from cellulosic biomass feedstock, in order to generate high-value products from wastes.

Acknowledgments

The authors acknowledge Universidad Nacional del Sur and Agencia Nacional de Promoción Científica y Tecnológica (ANPCyT, PICT-2370), SECYT-UNC, CONICET for their financial support. M. L. Nieva Lobos and V. Comignani are fellows of CONICET. Authors also thank Dr. Raúl Carbonio and Mr. Alejandro Mensaque for their ongoing assistance in the TG/DTG experiments.

REFERENCES

[1] a)Brown TR, Wright MM, Brown RC. Estimating profitability of two biochar production scenarios: slow pyrolysis vs fast pyrolysis. Biofuels Bioprod Biorefin 2011;5:54–68.
b)Antal MJ, Grønli M. The art, science and technology of charcoal production. Int Eng Chem Res 2003;42:1619–40.
c)Meyer S, Glaser B, Quicker P. Technical, economical, and climate-related aspects of biochar production technologies: a literature review. Environ Sci Technol 2011;45:9473–83.

[2] Kezhen Q, Ajay K, Hailin Z, Danielle B, Raymond H. Recent advances in utilization of biochar. Ren Sust En Rev 2015;42:1055–64.

[3] a)Wang S, Wang H, Yin Q, Zhu L, Yin S. Methanation of biosyngas over a biochar supported catalyst. New J Chem 2014;38:4471–7.
b)Zhu L, Yin S, Yin Q, Wang H, Wang S. Biochar: a new promising catalyst support using methanation as a probe reaction. Energy Sci Eng 2015;3(2):126–34.

[4] Nieva ML, Volpe MA, Moyano EL. Catalytic and catalytic free process for cellulose conversion: fast pyrolysis and microwave induced pyrolysis studies. Cellulose 2015;22(1):215–28.

[5] a)Xiao Z, Jianbing Z, Liang L, Chenyang L, Changpeng L, Jianhui L, et al. Biomass-derived N-doped carbon and its application in electrocatalysis. Appl Catal B Env 2014;154–155:177–82.
b)Huijuan Y, Hui W, Shan J, Yanjiao M, Linkov V, Rongfang W. Nanostructured Pt supported on cocoon-derived carbon as an efficient electrocatalyst for methanol oxidation. J Solid State Electrochem 2014;18:1503–12.

[6] a)Chuanlong H, Shiping W, Jing W, Mingming L, Jiang D, Haoran L, et al. Controlled synthesis of sustainable N-doped hollow core-mesoporous shell carbonaceous nanospheres from biomass. Nano Res 2014;7:1809–19.
b)Chao-Zhong Guoa, Wen-Li Liao, Chang-Guo C. Design of a non-precious metal electrocatalyst for alkaline electrolyte oxygen reduction by using soybean biomass as the nitrogen source of electrocatalytically active center structures. J Power Sources 2014;269:841–7.

[7] Hu Y, Wu P, Yin Y, Zhang H, Cai C. Effects of structure, composition, and carbon support properties on the electrocatalytic activity of Pt-Ni-graphene nanocatalysts for the methanol oxidation. Appl Catal B 2012;111–112:208–17.

[8] Jia JC, Wang RF, Wang H, Ji S, Key J, Linkov V, et al. A novel structural design of CNx-Fe_3O_4 as support to immobilize Pd for catalytic oxidation of formic acid. Catal Commun 2011;16:60–3.

[9] Vielstich W, Lamm A, Gasteiger HA, editors. Handbook of fuel cells-fundamentals, technology and applications2. New York: John Wiley & Sons; 2003.

[10] Watanabe M, Uchida H. Electrocatalysis at platinum and bimetallic alloys. In: Koper MTC, editor. Fuel cell catalysis. New Jersey: John Wiley & Sons; 2009.
[11] Celorrio V, Calvillo L, Moliner R, Pastor E, Lázaro MJ. Carbon nanocoils as catalysts support for methanol electrooxidation: a differential electrochemical mass spectrometry (DEMS) study. J Power Sources 2013;239:72–80.
[12] Alegre C, Baquedano E, Gálvez ME, Moliner R, Lázaro MJ. Tailoring carbon xerogels' properties to enhance catalytic activity of Pt catalysts towards methanol oxidation. Int J Hydrogen Energy 2015;40:14736–45.
[13] Calderón JC, Mahata N, Pereira MFR, Figueiredo JL, Fernándes VR, Rangel CM, et al. Pt-Ru catalysts supported on carbon xerogels for PEM fuel cells. Int J Hydrogen Energy 2012;37:7200–11.
[14] Calderón JC, García G, Calvillo L, Rodríguez JL, Lázaro MJ, Pastor E. Electrochemical oxidation of CO and methanol on Pt–Ru catalysts supported on carbon nanofibers: the influence of synthesis method. Appl Catal B 2015;165:676–86.
[15] Sebastián D, Lázaro MJ, Moliner R, Suelves I, Aricó AS, Baglio V. Oxidized carbon nanofibers supporting PtRu nanoparticles for direct methanol fuel cells. Int J Hydrogen Energy 2014;39:5414–23.
[16] Habibi B, Dadashpour E. Carbon-ceramic supported bimetallic Pt-Ni nanoparticles as an electrocatalyst for electrooxidation of methanol and ethanol in acidic media. Int J Hydrogen Energy 2013;38:5425–34.
[17] Chen M, Lou B, Ni Z, Xu B. PtCo nanoparticles supported on expanded graphite as electrocatalyst for direct methanol fuel cell. Electrochim Acta 2015;165:105–9.
[18] Wang L, Tian C, Zhang H, Fu H. Graphitic carbon nanocapsules: scaled preparation, formation mechanism, and use as an excellent support for methanol electro-oxidation. Eur J Inorg Chem 2012:961–8.
[19] Kakaei K, Zhiani M. A new method for manufacturing graphene and electrochemical characteristic of graphene-supported Pt nanoparticles in methanol oxidation. J Power Sources 2013;225:356–63.
[20] Liu M, Peng C, Yang W, Guo J, Zheng Y, Chen P, et al. Pd nanoparticles supported on three-dimensional graphene aerogels as highly efficient catalysts for methanol electrooxidation. Electrochim Acta 2015;178:838–46.
[21] Li K, Zhu J, Xiao M, Zhao X, Yao S, Liu C, et al. Promotion of mesoporous vanadium carbide incorporated on resorcinol–formaldehyde resin carbon composites with high-surface-areas on platinum catalysts for methanol electrooxidation. Chem Cat Chem 2014;6:3387–95.
[22] Jang YJ, Jang YH, Han S-B, Khatua D, Hess C, Ahn H, et al. Nanostructured metal/carbon hybrids for electrocatalysis by direct carbonization of inverse micelle multilayers. ASC Nano 2013;7:1573–82.
[23] Ioelovitch M, Tupureine A, Veveris G. Investigation of the crystalline structure of cellulose in plant materials. Khimija Drev 1989;5:3–9.
[24] Casoni A, Nievas ML, Moyano EL, Álvarez M, Diez A, Dennehy M, et al. Catalytic pyrolysis of cellulose using MCM-41 type catalysts. App Catal A 2016;514:235–40.
[25] Sieben JM, Alvarez AE, Comignani V, Duarte MME. Methanol and ethanol oxidation on carbon supported nanostructured Cu core Pt-Pd shell electrocatalysts synthesized via redox displacement. Int J Hydrogen Energy 2014;39:11547–56.
[26] Sieben JM, Duarte MME, Mayer CE. Supported Pt and Pt-Ru catalysts prepared by potentiostatic electrodeposition for methanol electrooxidation. J Appl Electrochem 2008;38:483–90.
[27] Dobele G, Meier D, Faix O, Radtke S, Rossinskaya G, Telysheva G. Volatile products of catalytic flash pyrolysis of celluloses. J Anal Appl Pyrol 2001;58:453–63.
[28] Zhang J, Zhang J, Lin L, Chen T, Zhang J, Liu S, et al. Dissolution of microcrystalline cellulose in phosphoric acid-molecular changes and kinetics. Molecules 2009;14:5027–41.
[29] Zhao H, Kwak J, Zhang Z, Brown H, Arey B, Holladay J. Studying cellulose fiber structure by SEM, XRD, NMR and acid hydrolysis. Carbohydr Polym 2007;68:235–41.
[30] Carpenter D, Westover TL, Czernika S, Jablonskia W. Biomass feedstocks for renewable fuel production: a review of the impacts of feedstock and pretreatment on the yield and product distribution of fast pyrolysis bio-oils and vapors. Green Chem 2014;16:384–406.
[31] Yu JT, Dehkhoda AM, Ellis N. Development of biochar-based catalyst for transesterification of canola oil. Energy Fuels 2011;25:337–44.
[32] a)Dehkhoda AM, West AH, Ellis N. Biochar based solid acid catalyst for biodiesel production. Appl Catal A 2010;382:197–204.
b)Yan Q, Wan C, Liu J, Gao J, Yu F, Zhang J. Iron nanoparticles in situ encapsulated in biochar based carbon as an effective catalyst for the conversion of biomass-derived syngas to liquid hydrocarbons. Green Chem 2013;15:1631–40.
[33] Tam MS, Antal Jr MJ, Jakab EB, Várhegyi G. Activated carbon from macadamia nut shell by air oxidation in boiling water. Ind Eng Chem Res 2001;40:578–88.
[34] Sieben JM, Duarte MME, Mayer CE. Electro-oxidation of methanol on PtRu nanostructured catalysts electrodeposited onto electroactivated carbon fiber materials. Chem Cat Chem 2010;2:182–9.
[35] Sieben JM, Ansón-Casaos A, Martínez MT, Morallón E. Single-walled carbon nanotube buckypapers as electrocatalyst supports for methanol oxidation. J Power Sources 2013;242:7–14.
[36] Warren BE. X-Ray diffraction. Massachusetts: Addison-Wesley; 1969. Reading.
[37] Sieben JM, Comignani V, Alvarez AE, Duarte MME. Int J Hydrogen Energy 2014;39:8667–74.
[38] Shibata T, Bunker BA, Zhang Z, Meisel D, Vardeman CF, Gezelter J. Size-dependent spontaneous alloying of au-ag nanoparticles. J Am Chem Soc 2002;124:11989–96.
[39] Cherstiouk OV, Simonov PA, Savinova ER. Model approach to evaluate particle size effects in electrocatalysis: preparation and properties of Pt nanoparticles supported on GC and HOPG. Electrochim Acta 2003;48:3851–60.
[40] Strasser P, Koh S, Anniyev T, Greeley J, More K, Yu C, et al. Lattice-strain control of the activity in dealloyed core–shell fuel cell catalysts. Nat Chem 2010;2:454–60.
[41] Goto S, Hosoi S, Arai R, Tanaka S, Umeda M, Yoshimoto M, et al. Particle-size- and Ru-core-induced surface electronic states of Ru-core/Pt-shell electrocatalyst nanoparticles. J Phys Chem C 2014;118:2634–40.
[42] Alayoglu S, Nilekar AU, Mavrikakis M, Eichhorn B. Ru–Pt core–shell nanoparticles for preferential oxidation of carbon monoxide in hydrogen. Nat Mater 2008;7:333–8.
[43] Chen T-Y, Luo T-JM, Yang Y-W, Wei Y-C, Wang K-W, Lin T-L, et al. Core dominated surface activity of core-shell nanocatalysts on methanol electrooxidation. J Phys Chem C 2012;116:16969–78.
[44] Jiang J, Kucernak A. Electrooxidation of small organic molecules on mesoporous precious metal catalysts II: CO and methanol on platinum/ruthenium alloy. J Electroanal Chem 2003;543:187–99.
[45] Gasteiger HA, Kocha SS, Sompalli B, Wagner FT. Activity benchmarks and requirements for Pt, Pt-alloy, and non-Pt oxygen reduction catalysts for PEMFCs. Appl Catal 2005;56:9–35.
[46] Chrzanowaki W, Wieckowski A. In: Wieckowski A, editor. Interfacial electrochemistry: theory, experiment, applications. New York: Marcel Dekker; 1999. p. 950.

[47] Hsieh CT, Gu JL, Tzou DY, Chu YC, Chen YC. Microwave deposition of Pt catalysts on carbon nanotubes with different oxidation levels for formic acid oxidation. Int J Hydrogen Energy 2013;38:10345–53.
[48] Antonucci PL, Alderucci V, Giordano N, Cocke DL, Kim H. On the role of surface functional groups in Pt carbon interaction. J Appl Electrochem 1994;24:58–65.
[49] Alegre C, Calvillo L, Moliner R, González-Expósito JA, Guillén-Villafuerte O, Martínez Huerta MV, et al. Pt and PtRu electrocatalysts supported on carbon xerogels for direct metanol fuel cells. J Power Sources 2011;196:4226–35.
[50] Kim JH, Kwon SY, Bhattacharjya D, Chai GS, Yu J-S. High-performance quaternary PtRuIrNi electrocatalysts with hierarchical nanostructured carbon support. J Catal 2013;306:133–45.
[51] Zhang Y, Zhu R, Cui Y, Zhong J, Zhang X, Chen J. Pt, Ru nanoparticles supported on nitrogen-doped polyhedral mesoporous carbons as electrocatalyst for methanol oxidation. Nanotechnology 2014;25:135–607.
[52] Su F, Poh CK, Tian Z, Xu G, Koh G, Wang Z, et al. Electrochemical behavior of pt nanoparticles supported on meso- and microporous carbons for fuel cells. Energy Fuels 2010;24:3727–32.
[53] Liu Z, Su F, Zhang X, Tay SW. Preparation and characterization of PtRu nanoparticles supported on nitrogen-doped porous carbon for electrooxidation of methanol. ACS Appl Mater Interfaces 2011;3:3824–30.
[54] Su F, Tian Z, Poh CK, Wang Z, Lim SH, Liu Z, et al. Pt nanoparticles supported on nitrogen-doped porous carbon nanospheres as an electrocatalyst for fuel. Cells Chem Mater 2010;22:832–9.
[55] Sebastián D, Suelves I, Pastor E, Moliner R, Lázaro MJ. The effect of carbon nanofiber properties as support for PtRu nanoparticles on the electrooxidation of alcohols. Appl Catal B 2013;132–133:13–21.
[56] Kuo CW, Lu IT, Chang LC, Hsieh YC, Tseng YC, Wu PW, et al. Surface modification of commercial PtRu nanoparticles for methanol electro-oxidation. J Power Sources 2013;240:122–30.
[57] Zhou T, Wang H, Feng H, Wang R. Synthesis of mesoporous carbon from Okara and application as electrocatalyst support. Fuel Cells 2014;14:296–302.
[58] Fan Y, Liu PF, Yang ZJ, Jiang TW, Yao KL, Han R, et al. Bi-functional porous carbon spheres derived from pectin as electrode material for supercapacitors and support material for Pt nanowires towards electrocatalytic methanol and ethanol oxidation. Electrochim Acta 2015;163:140–8.